SCIENTIFIC REPORTS

OPEN

SUBJECT AREAS:
COLON CANCER
BIOMARKER RESEARCH
APPLIED MICROBIOLOGY

Received
13 January 2014

Accepted
28 April 2014

Published
15 May 2014

Correspondence and requests for materials should be addressed to S.L. (shaoli@mail.tsinghua.edu.cn)

* These authors contributed equally to this work.

Dynamic microbe and molecule networks in a mouse model of colitis-associated colorectal cancer

Xujun Liang[1]*, Huiying Li[1]*, Geng Tian[2] & Shao Li[1,3]

[1]MOE Key Lab of Bioinformatics, Bioinformatics Division, TNLIST and Department of Automation, Tsinghua University, Beijing 100084, China, [2]Center of Biomedical Analysis, Tsinghua University, Beijing 100084, China, [3]School of Medicine/School of Life Sciences, Tsinghua University, Beijing 100084, China.

Bacterial colonisation of the gut is involved in the development of colitis-associated colorectal cancer. However, it remains unclear how the gut microbiota dynamically shifts correlating with colorectal carcinogenesis. Here, we reveal the longitudinal shifts in the microbial community that occur with colitis-associated colorectal cancer. High-throughput sequencing results for the bacterial 16S rRNA gene (V3 region) were compared for azoxymethane/dextran sodium sulphate-treated mice and control mice. We found that microbial community structure was significantly altered by chronic colitis. Microbes in the species *Streptococcus luteciae*, *Lactobacillus hamster*, *Bacteroides uniformis* and *Bacteroides ovatus* were increased during colorectal carcinogenesis. Histological measurements for a molecular network including six interconnected key factors from inflammation to cancer, namely p65, p53, COX-2, PPARγ, CCR2 and β-catenin, indicated that the microbiome modifications were correlated with molecular pathogenesis of colitis-associated colorectal cancer. Phylotype modifications after each AOM/DSS cycle were identified. A longitudinal microbial network was then constructed for the gut microbiome and showed that the phylotype shifts during this process were complex and highly dynamic. This work may provide a deeper understanding of the role of the microbiota and microbe-host interactions in colitis-associated colorectal cancer.

Experimental and clinical studies have frequently suggested that chronic inflammation is an important factor related to carcinogenesis[1]. Colorectal cancer is one cancer for which a relationship with chronic inflammation has been well established. It has been reported that individuals with inflammatory bowel disease (IBD) are at increased risk for colorectal cancer[2,3]. The mechanisms by which chronic intestinal inflammation promotes colorectal cancer have not been fully elucidated, but persistent exposure to inflammatory mediators and repeated damage/repair cycles are believed to contribute to the development of epithelial cell-associated cancer[4,5].

For cancers that are associated with inflammation, the microbiota is thought to be an important source of infection and a carcinogenic factor[6]. It was reported that some strains in *Bacteroides fragilis* and *Escherichia coli*, were enterotoxigenic and directly promoted tumourigenesis[7,8]. In the colon, the microbiota is comprised of 10^{14} prokaryotes and 10^{3} different species[9]. The colonic microbiota is critical for mucosal tolerance under normal conditions and prevents pathogen infections[10,11]. However, recent studies have shown that the colonic microbiota can promote or aggravate chronic inflammation in the intestine[11]. There is also increased evidence indicating that breakdown of the intestinal microbiota structure is associated with colon cancer[12–15]. Thus, it is important to describe alterations to the intestinal microbiota during chronic intestinal inflammation and colitis-associated colorectal cancer.

Structural changes to microbial communities are studied by various methods. One method that has been widely used in recent studies is the 16S rRNA gene sequencing approach. This approach provides an effective method with which to globally analyse a microbial community and identify specific phylotypes as biomarkers[16,17]. Using the 16S rRNA sequencing approach, previous studies have shown that the gut microbiota structure is different between IBD patients and healthy controls[18,19]. A more recent study that combined 16S rRNA sequencing and whole genome analysis of the colorectal cancer microbiota reported a modification in the gut microbiota structure in colorectal cancer patients and associated *Fusobacterium* with colorectal cancer[20]. These works provide large-scale descriptions of changes to the structure of the gut microbiota in IBD and colorectal cancer and demonstrate that gut microbial changes are closely related to these diseases, but further studies are still necessary to uncover the role the microbiota plays as gut inflammation progresses to colorectal cancer.

In addition to analysing clinical samples from IBD and colorectal cancer patients, animal studies have also been performed to uncover the pathological effects of gut microbial dysbiosis. Mice given chronic treatment of dextran sulphate sodium (DSS) treatment develop intestinal inflammation, and this treatment effectively models IBD[21]. By performing 16S rRNA gene sequencing and metatranscriptomics surveys of DSS-treated mice, D. Berry *et al.* found a microbial community composition modification at the family level driven by DSS-induced colitis[22]. Using a genetic deficiency mouse model together with the colon-specific carcinogen azoxymethane (AOM), J. C. Arthur *et al.* demonstrated that inflammation altered gut microbial composition, and *Escherichia coli NC101* was specifically related to carcinogenesis[8]. Recently, Zackular *et al* utilized a AOM/DSS model and suggested that the time course changes of gut microbiome were directly related to tumourigenesis[23]. These studies show that animal models permit the effective study of microbial factors involved in the progression from IBD to cancer, and animal studies have revealed the important role of the gut microbiota in these diseases. However, details and a dynamic description of changes to the microbiota and the relationships among gut microbiome, host molecules are still few as inflammation develops into cancer. The microbial link between gut inflammation and cancer is unclear.

In this study, we employed a mouse model of colitis-associated cancer by combining DSS with AOM. By obtaining and sequencing mouse faecal samples after different cycles of AOM/DSS treatment, we developed a time-course study of the microbiota in colitis-associated cancer. First, histological measurements of p65, p53, COX-2, PPARγ, CCR2 and β-catenin, six molecules closely related to inflammation and cancer were carried out. Based on the results, a dynamic molecular network was constructed to reveal the pathological process in the animal model of colitis-associated colorectal cancer. Next, gut microbial community structures were compared between control mice and mice treated with AOM/DSS. Differences in gut microbial composition were found between control and treated animals. Third, the phylotypes underlying these differences were identified. The species *Streptococcus luteciae*, *Lactobacillus hamster*, *Bacteroides uniformis* and *Bacteroides ovatus* were significantly enriched in treatment group samples. The dynamic microbiome modifications were correlated with changes of tumour counts and the host dynamic molecular network. Finally, phylotype alterations were identified at different points along the time course. Longitudinal phylotype profiles were mined to characterise bacterial fluctuations during the development of colitis-associated cancer. Some profiles contained microbes that may promote inflammation and cancer. A network of microbial profiles was constructed to further reveal the relationships between the dynamic patterns of phylotype variations.

Results

Progression from chronic colitis to colorectal cancer in a mouse model and a dynamic molecule network. BALB/c mice were treated with AOM and different cycles of 3% DSS. It was observed that the inflammation-induced tissue damage began after the first AOM/DSS cycle and became more evident after 2 AOM/DSS cycles (Fig. S1A and Fig. S1B). Number of dysplasia and carcinoma were counted in the colons of mice after treatment with three more cycles of AOM/DSS (Fig. 1A). Next, to characterise the progression of chronic colitis-associated carcinogenesis at the molecular level, immunohistochemical staining for a molecule network consisted of p65, p53, COX-2, PPARγ, β-catenin and CCR2 was carried out. These molecules were ranked high on inflammation and cancer related gene list inferred by CIPHER method[24]. It also has been reported that these molecules are parts of main factors involved in colonic carcinogenesis[25,26], and they are also in close proximity to each other in a protein-protein interaction network (Fig. 1C). In untreated mice, both p53 and p65 staining was almost undetectable. After AOM/DSS treatment, the expression level of p53 and p65 was increased and p65 exhibited increased accumulation in the cell nucleus throughout the progression of carcinogenesis. The similar behaviors of p53 and the inflammatory factors were also detected in the DSS mouse model of colitis-induced cancer previously[27]. β-catenin was increased and translocated from the cell membrane to the cytoplasm and nucleus. The expressions of COX-2 and CCR2 were increased during the development from inflammation to colorectal dysplasia and cancer. It is reported that COX-2 is highly expressed in the DSS model of colitis-related cancer[27] and CCR2 is also activated in colon carcinomas[26]. We also noted that the expression of PPARγ in intestinal mucosa tissue and intestinal epithelial cells was elevated during this process (Fig. 1B). And it was reported that in the absence of an exogenous ligand, PPARγ in colonic epithelium has a protective effect against DSS-induced colitis, being embodied in the up-regulation of PPARγ[28]. The observed modifications of these molecules were quantified and visualized by dynamic molecule networks (Fig. 1C). The dynamic patterns of these molecules may imply regulatory relationships among them.

Diversity and structural changes of the microbiota community during colonic colitis-induced carcinogenesis. To study the diversity and structure of the intestinal microbiota community of the colitis-associated cancer murine model, 16S rRNA V3 region amplicon sequence libraries from faecal samples of AOM/DSS treated mice were sequenced. Sequencing gave approximately 22.9 million paired raw reads in total. The number of raw reads pairs and the number of sequences represented OTUs of each sample were shown in Table S1. These high quality sequences were clustered into OTUs at different genetic similarity levels (100%, 97% and 95%).

For alpha diversity analysis, rarefaction analysis was conducted for each sample. The rarefaction curves were constructed as the function of sequence counts to the number of OTUs observed (Fig. S2). Estimators of community richness, evenness and diversity were calculated based on the OTUs (97% similarity) (Fig. S3). We found that microbial richness was not changed by AOM/DSS treatment, while microbial diversity and evenness were significantly decreased in the model group mice with inflammation only (treated with one or two AOM/DSS cycles, Fig. S4).

For beta diversity analysis, the Jaccard similarity coefficient was calculated based on the OTUs (97% similarity) to compare microbial community membership between control mice and all mice treated with AOM/DSS. Community membership was impacted by AOM/DSS treatment, but the difference between the control and model groups was not significant (Fig. 2A, P-value = 0.07). The community membership of mice in the control group and mice in the model group with dysplasia and cancer was different, although this difference was not significant after multiple test correction (raw P-value = 0.046, P-value = 0.184 after Bonferroni correction). Next, to compare the microbial community structures of control mice and all mice treated with AOM/DSS, the Bray-Curtis similarity coefficient and the Yue & Clayton theta similarity coefficient were calculated. Both of these coefficients indicated that the microbial community structure as significant changed by AOM/DSS treatment (Fig. 2A). The mice in the inflammation-only model group and the mice in the model group with dysplasia and cancer exhibited no significant differences in both microbial community membership and microbial community structure. Sample clustering under different distance metrics as visualised by non-metric multidimensional scaling (NMDS) methods (Fig. 2B).

The relative abundances of phylum-level bacterial taxa were compared between control samples and samples from AOM/DSS-treated mice. As Fig. 3A and Fig. 3B shows, *Bacteroidetes* and *Firmicutes* were the dominant phyla in most mouse faecal samples, accounting for 22.7–85.2% and 8.99–62.8% of phyla, respectively, and 83.8–92.4% of phyla in total. *Cyanobacteria*, *Proteobacteria*, *Tenericutes*,

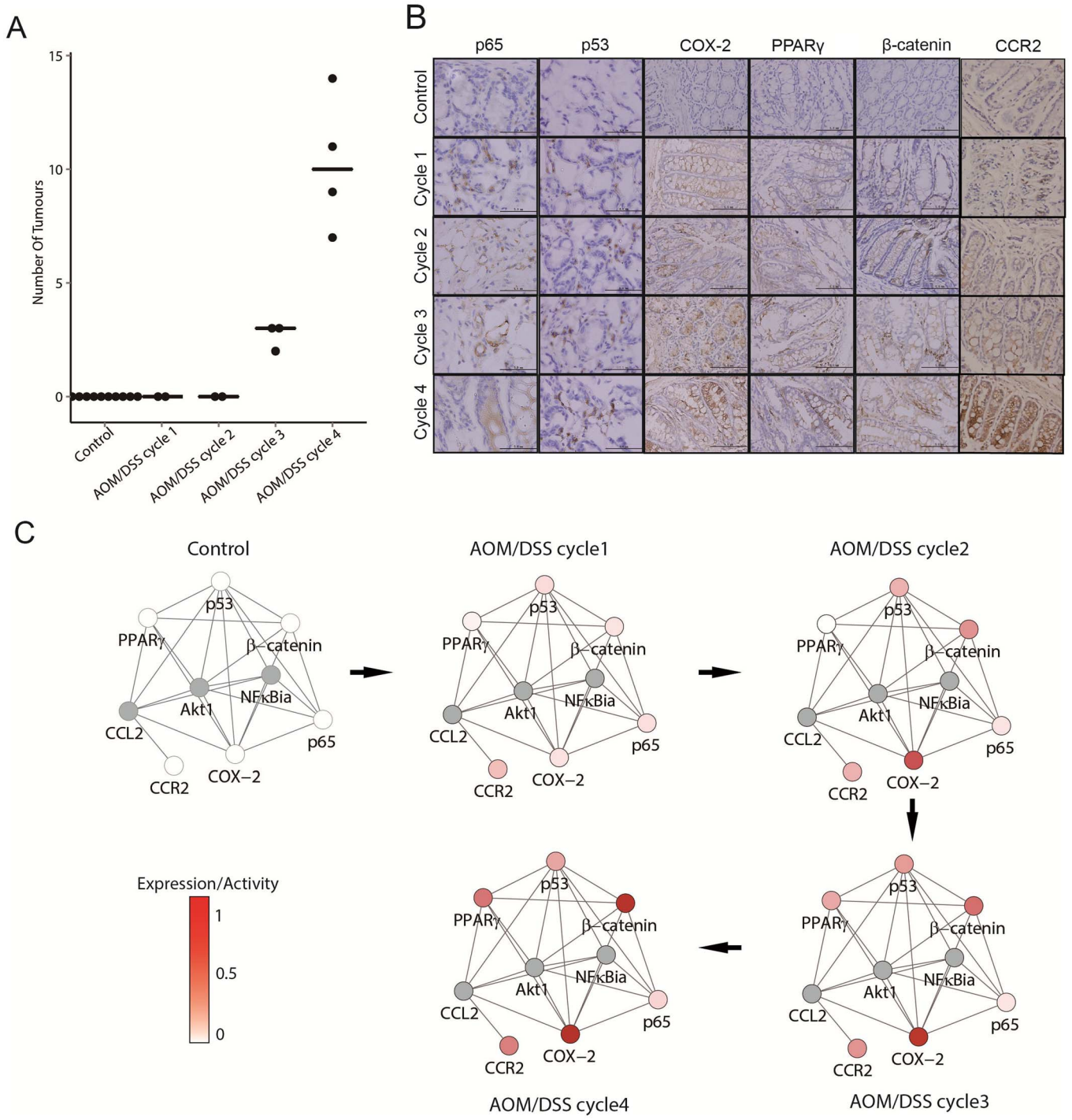

Figure 1 | Representative staining for molecular markers involved in the progression of chronic colitis-associated carcinogenesis. (A) Mice treated with 1–4 AOM/DSS cycles were euthanized then the numbers of tumors in the colons were counted. Tumors were found in mice treated with 3–4 AOM/DSS cycles. Black bars are medians of each group. (B) Representative staining for six molecules reflects the pathological progression of chronic colitis and carcinogenesis. Rows represent the control group and mice treated with different AOM/DSS cycles. (C) The molecular markers examined are closely related in the protein-protein interaction (PPI) network. The dynamic changes in the expression levels (trans-nuclear rate for p65) of the molecular markers were quantified and represented by colour scale. Grey nodes are linker genes in the PPI and not for testing.

Actinobacteria, *Verrucomicrobia* and *Synergistetes* for the most part constituted the rest of the gut microbiome in our samples (Fig. 3B and Fig. 3C). There were also some sequences that were bacterial but were not aligned to any taxonomic group by the methods we used. The less abundant phyla, i.e., with relative abundances $< 10^{-4}$%, are shown in Fig. 3C and Fig. 3D. When comparing the relative abundance of phyla between the control group and the AOM/DSS-treated group, we found that the relative abundance of *Bacteroidetes* and *Firmicutes* in the control group was not significantly different from the AOM/DSS-treated group (Fig. 3A). The other phyla that were consistently detected also did not change significantly. Among the rare phyla, *Chlorobi* was rarely present in the control group (6.25E-07% on average) but increased with increased numbers of AOM/DSS cycles (3.44E-06% in mice treated with 1–2 AOM/DSS cycles, 3.00E-05% in mice treated with 3–4 AOM/DSS cycles, shown in Fig. 3C).

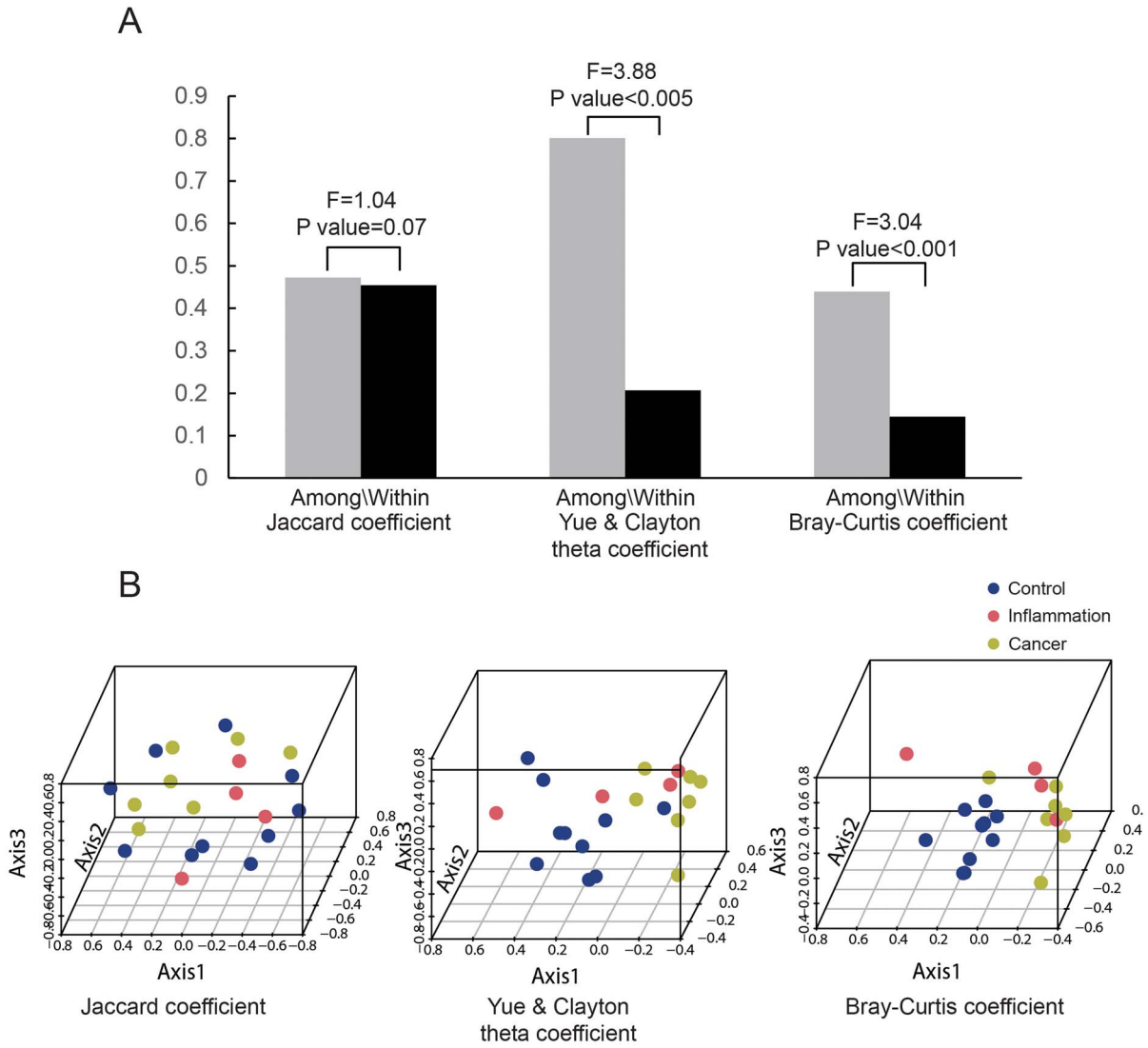

Figure 2 | Shifts in microbial community structure induced by chronic AOM/DSS treatment. (A) AMOVA results for the between-sample Jaccard coefficient, the Yue & Clayton theta coefficient and the Bray-Curtis coefficient for the control group and AOM/DSS-treated group. The F-statistic is the ratio of the mean square among the groups and within the groups. (B) NMDS plots of samples with different distance metrics indicate the separation between control and treated groups. Mice with inflammation only and mice with tumours are not separated. Colours represent different mouse groups. Blue: control group. Red: Mouse group treated with 1–2 AOM/DSS cycles, only inflammation observed. Yellow: Mouse group treated with 3–4 AOM/DSS cycles, with observed dysplasia and carcinoma.

Identification of phylotypes related to inflammation and cancer. As the above results show, the microbiota community structure of the colitis-associated cancer murine model changed, but phylum-level bacterial taxa were not greatly affected by AOM/DSS treatment. Therefore, an analysis was performed based on the 97% similarity OTU to determine whether a more specific phylotype difference existed between the control and the treated mice. After filtering out the OTUs with very low counts, 467 97% OTUs remained for further study. A multidimensional scaling plot (MDS) was drawn according to log-fold-changes distances between samples (Fig. 4A). The control group samples and AOM/DSS treated group samples separated clearly along the second dimension. Next, using an exact test, 70 97% OTUs were found to be significantly different between the control group and the AOM/DSS-treated group (Fig. 4b and Table S2, FDR < 0.05). Among these OTUs, 31 were higher and 39 were lower in the model group treated with AOM/DSS. Two OTUs belonging to species *Streptococcus luteciae* (OTU01779, FDR $= 0.015$) and *Lactobacillus hamster* (OTU00907, FDR $= 0.035$) were significantly higher in the model group samples. Two OTUs frome genus *Bacteroides*, OTU00082 (classified as *Bacteroides uniformis*) and OTU00363 (classified as *Bacteroides ovatus*) were also significantly enriched in model group samples (Fig. 4B, Table S2); while three OTUs affiliated to genus *Oribacterium* (OTU00441, OTU00062, OTU00157) were enriched in samples from the control group (Table S2). These phylotypes could be considered as biomarkers to separate normal mice from mice with colitis or colon cancer.

We also investigated whether there were phylotypes that were differentially enriched between mice with inflammation only and mice that developed dysplasia and cancer. The results showed that 9 OTUs were more abundant in mice with inflammation only, and one OUT was more abundant in mice with cancer (Table. S3). Fig. 4C shows three of these OTUs that were most abundant in samples from model group mice. OTU00491 (unclassified *Erysipelotrichaceae*) and OTU00024 (genus *Bacteroides*) were significantly abundant in the AOM/DSS-treated group (FDR < 0.05) and more abundant in mice with inflammation only than in mice with dysplasia and cancer. OTU00023 (unclassified S24-7) was significantly less abundant in

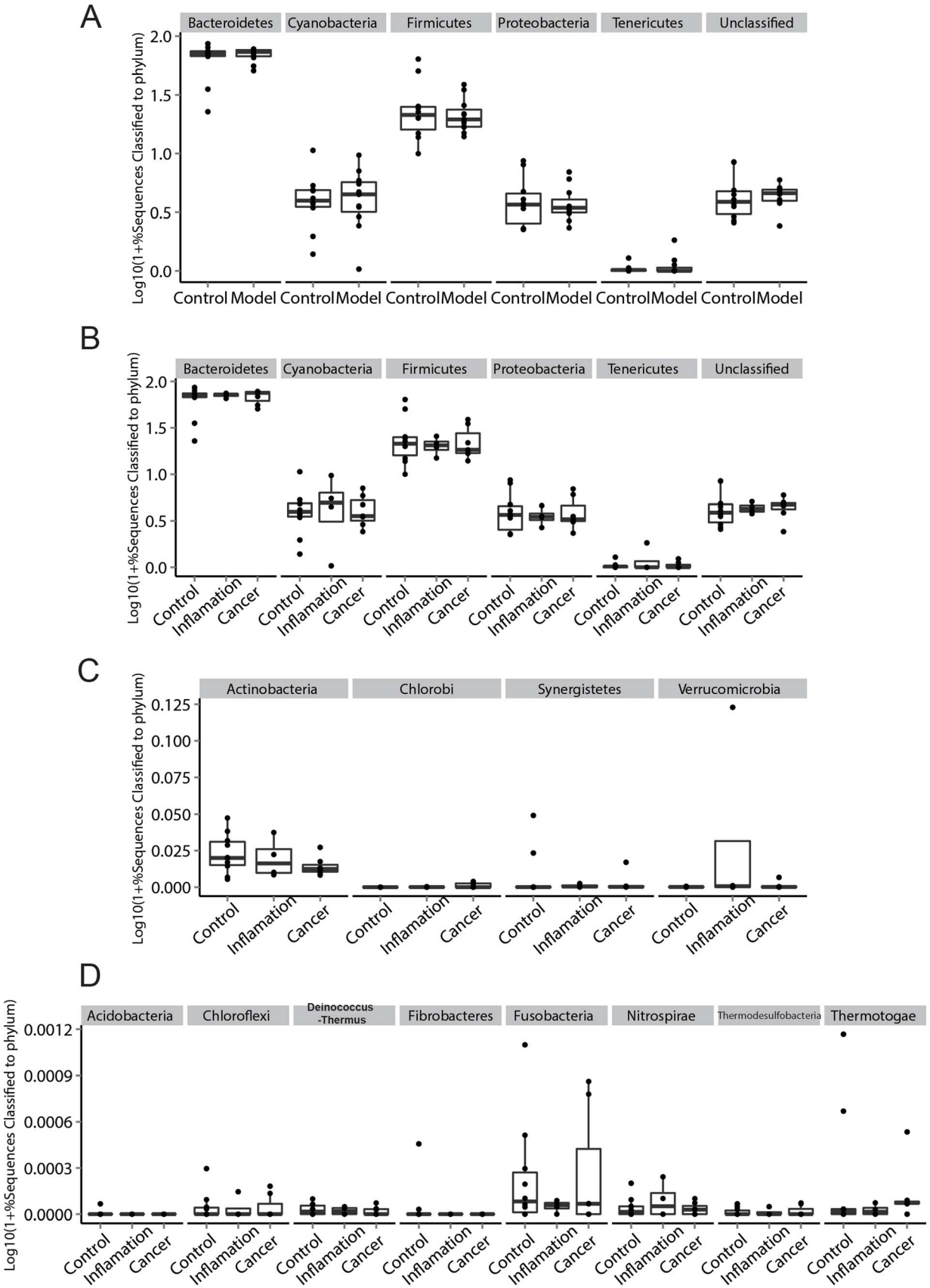

Figure 3 | Taxonomy classification of the mouse gut microbiome at the phylum level. (A) Relative abundances of the dominant phyla in samples of control group and model group. (B)–(D) Relative abundances of all phyla for mice in control group, group only with inflammation and group with tumour. (B) Relative abundances of dominant phyla and unclassified sequences. (C) Relative abundances of moderately abundant phyla (D) Relative abundances of rare phyla.

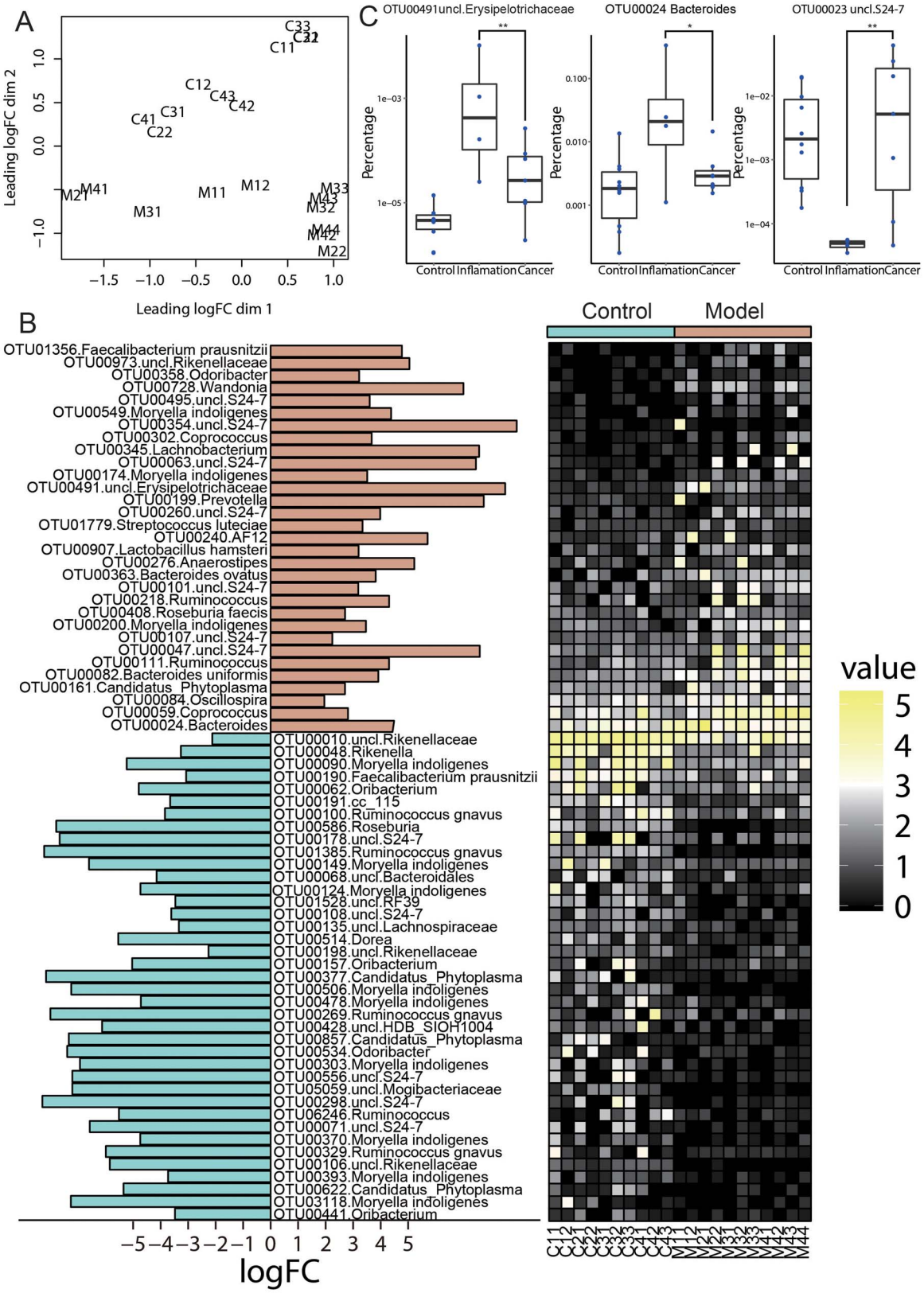

Figure 4 | Significant differential OTUs in the control group and AOM/DSS treated group. (A) Multidimensional scaling (MDS) plot, based on log-fold-changes distances between samples. (B) Log-fold-change and heat map of significantly differential OTUs (FDR < 0.05). (C) The three most abundant differential OTUs between mice with inflammation only and mice that developed dysplasia and cancer. *, FDR < 0.05, **, FDR < 0.01. "uncl" means unclassified. In (A) and (B), each sample was denominated as follows: the beginning C/M represents the control or model group; the middle number represents the number of AOM/DSS cycles for the model group or the euthanisation batch for the control group; the last number represents different mice for repeats.

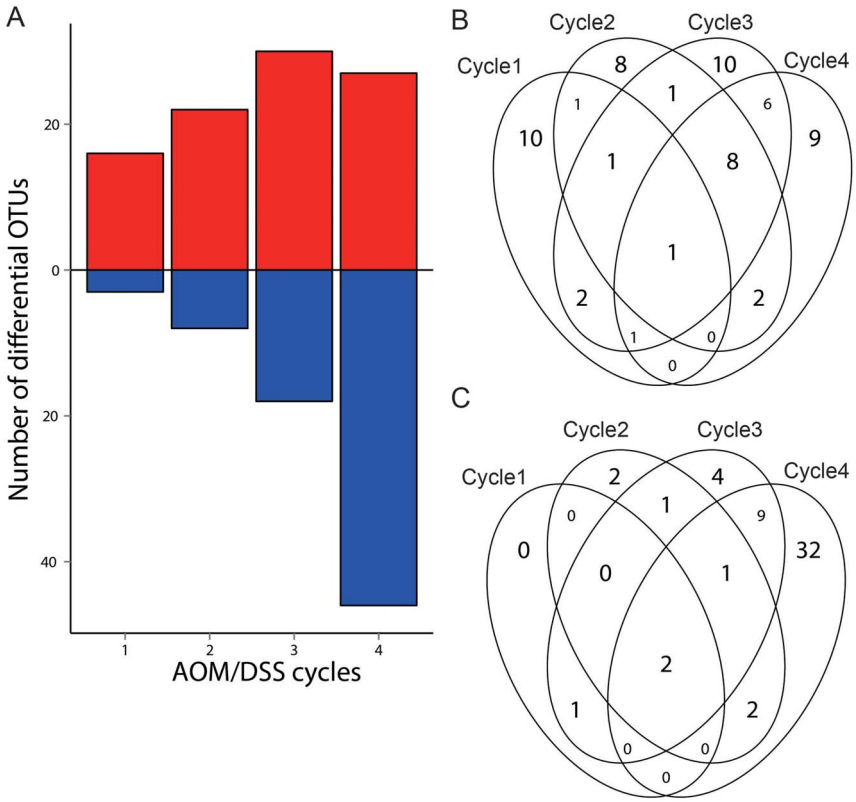

Figure 5 | The number of differential OTUs during the development of colitis-associated cancer. (A) The number of significantly increased OTUs (red) and decreased OTUs (blue) of mice treated with different AOM/DSS cycles compared to control mice (FDR < 0.05). Venn diagrams indicate the number of overlapping differential OTUs between mice with different AOM/DSS cycles: (B) increased OTUs, (C) decreased OTUs.

mice with inflammation only than in control mice and mice with dysplasia and cancer (FDR = 1.71E-05) but exhibited no difference between the latter two groups.

To identify which phylotypes were closely related to tumour occurrence, correlations between tumour counts and relative abundances of 97% OTUs (after filtering the low abundant OTUs) were calculated. 37 OTUs were observed significantly related to the colonic tumour counts of mice after different AOM/DSS cycles (P-value < 0.05, Table S6). Many of these OTUs classified as species *Moryella indoligenes, Ruminococcus gnavus*. Furthermore, the molecules measured in Fig. 1 reflected the developmental process of inflammation to colon cancer. We also explored correlations between changes of host molecular activity or expression with microbial community modifications. Some OTUs' changes were significantly correlated with host molecular expression or activity (Table S7). A dynamic network was constructed to visualize the coordinated changes of molecules and OTUs (Fig. S6). We observed that some OTUs significantly negatively related to the host molecule changes, such as OTUs affiliated to genus *Oxobacter*, species *Roseburia faecis* and *Flexithrix dorotheae*. These results suggest that some gut taxa were closely related to the development process of colitis to colorectal cancer and the dynamic patterns of these taxa could be important.

Time course of differential OTUs across various AOM/DSS cycles and a dynamic network of OTU profiles. As Fig. 1 and previous studies indicated[29,30], the development of colorectal cancer from inflammation is progressive and time-dependent. We next sought to reveal changes in OTUs after different AOM/DSS cycles across this progressive time course. After filtering OTUs with low abundance, a total of 19, 30, 48 and 73 OTUs were found to be significantly different between control mice and mice with AOM/DSS treatment after 1, 2, 3 and 4 cycles (FDR < 0.05), respectively. Detailed information for these differential OTUs is shown in Table S4. The numbers of the increased and decreased OTUs are shown in Fig. 5A. Both the number of increased and decreased OTUs became higher as the number of AOM/DSS cycles increased with the exception of the number of increased OTUs after AOM/DSS cycle 4, and this trend was more obvious for decreased OTUs. Furthermore, both increased and decreased OTUs exhibited significant overlaps between successive AOM/DSS treatment cycles (FDR < 0.05, Fig. 5B and Fig. 5C). This indicates that modification of the microbial community via AOM/DSS treatment is closely related to pathological progression.

To stringently analyze the longitudinal microbiota community changes stringently, we employed STEM (Short Time Expression Miner)[31], a strategy which was previously used to analyze time course microarray expression data to mine the OTU profiles. First, a set of 30 model profiles with five points was generated, and then each OTU was assigned to a profile. The 10 most enriched profiles comprised 55.7% of all OTUs assigned to the 30 profiles. Three profiles were significantly enriched for OTUs that longitudinally varied during AOM/DSS cycles (Fig. 6A). Changes in OTU abundance for the four most enriched profiles (profile 28, profile 12, profile 20 and profile 11) are depicted in Fig. 6B. Profile 28 is the most enriched profile; it exhibits a spike after 1–2 AOM/DSS cycles and a decrease to baseline or lower levels after 3–4 AOM/DSS cycles. More details about the OTU profiles are provided in Table S5.

For most profiles, it was observed that OTUs in same profile were significantly associated in lineages than random background (Fig. S5 and Table S8). We assumed that OTUs in the same profile shared overlapping niches. The OTUs in the same profile may represent a group of taxa which are functionally related and ecological coherent. We constructed a network to reveal the relationships between profiles to explore the possible interaction between these bacterial groups (Fig. 7). The profiles showed different correlation relationships with each other. It was observed that some profiles with nega-

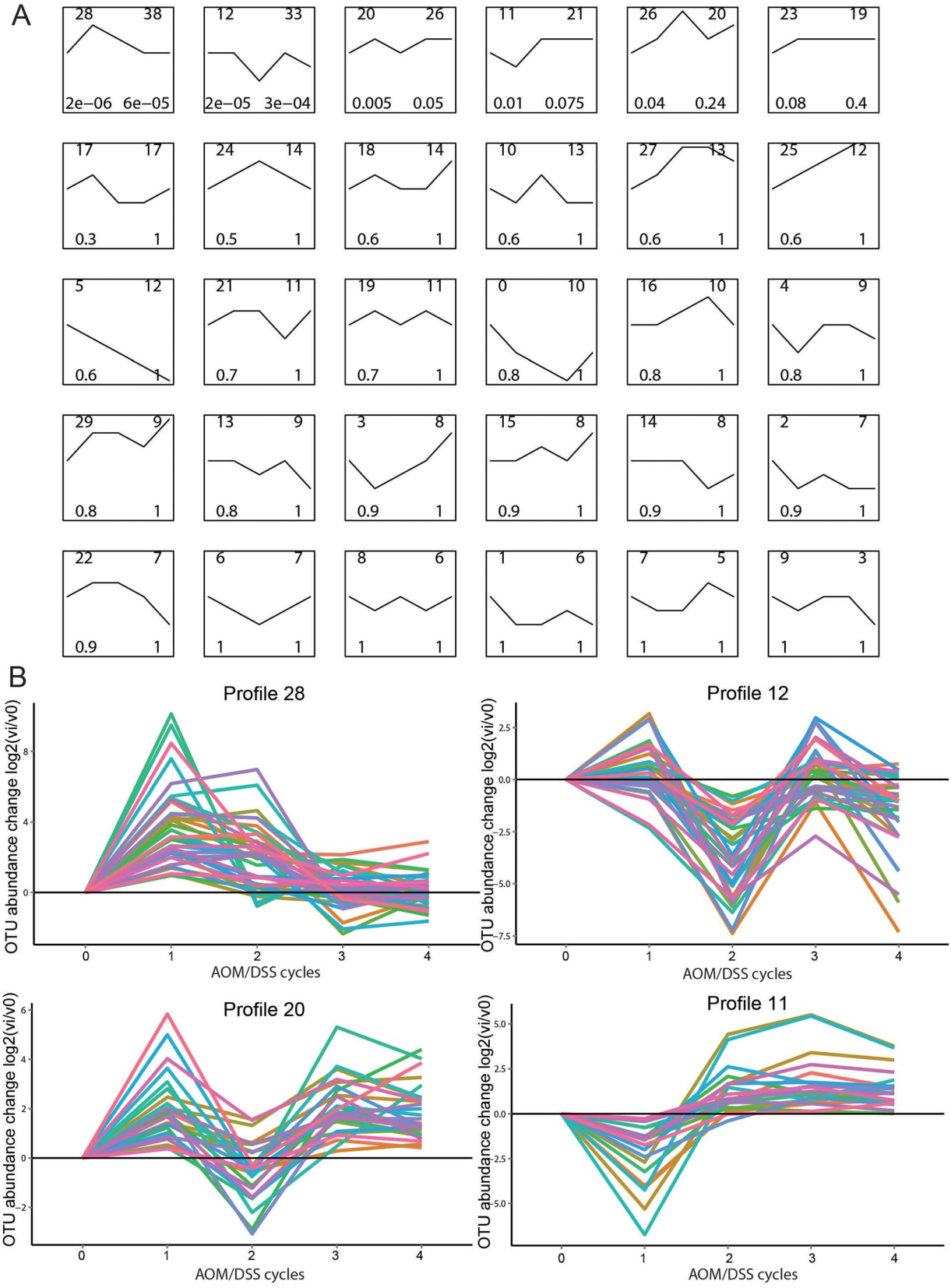

Figure 6 | Longitudinal profiles of OTUs reveal the dynamic patterns of microbial fluctuation during colitis-associated colorectal cancer. (A) Lines represent OTU relative abundance patterns across the five groups: the control group and the groups treated with 1–4 AOM/DSS cycles. The numbers in the upper-left corners are the serial numbers of the profiles. The numbers in the upper-right corners are the numbers of OTUs assigned to the profiles. The numbers in the lower-left corners are the raw P-values representing significance of overrepresentation. The numbers in the lower-right corners are the P-values adjusted by FDR. (B) The four profiles with the greatest overrepresentation; different OTUs are depicted with different colours.

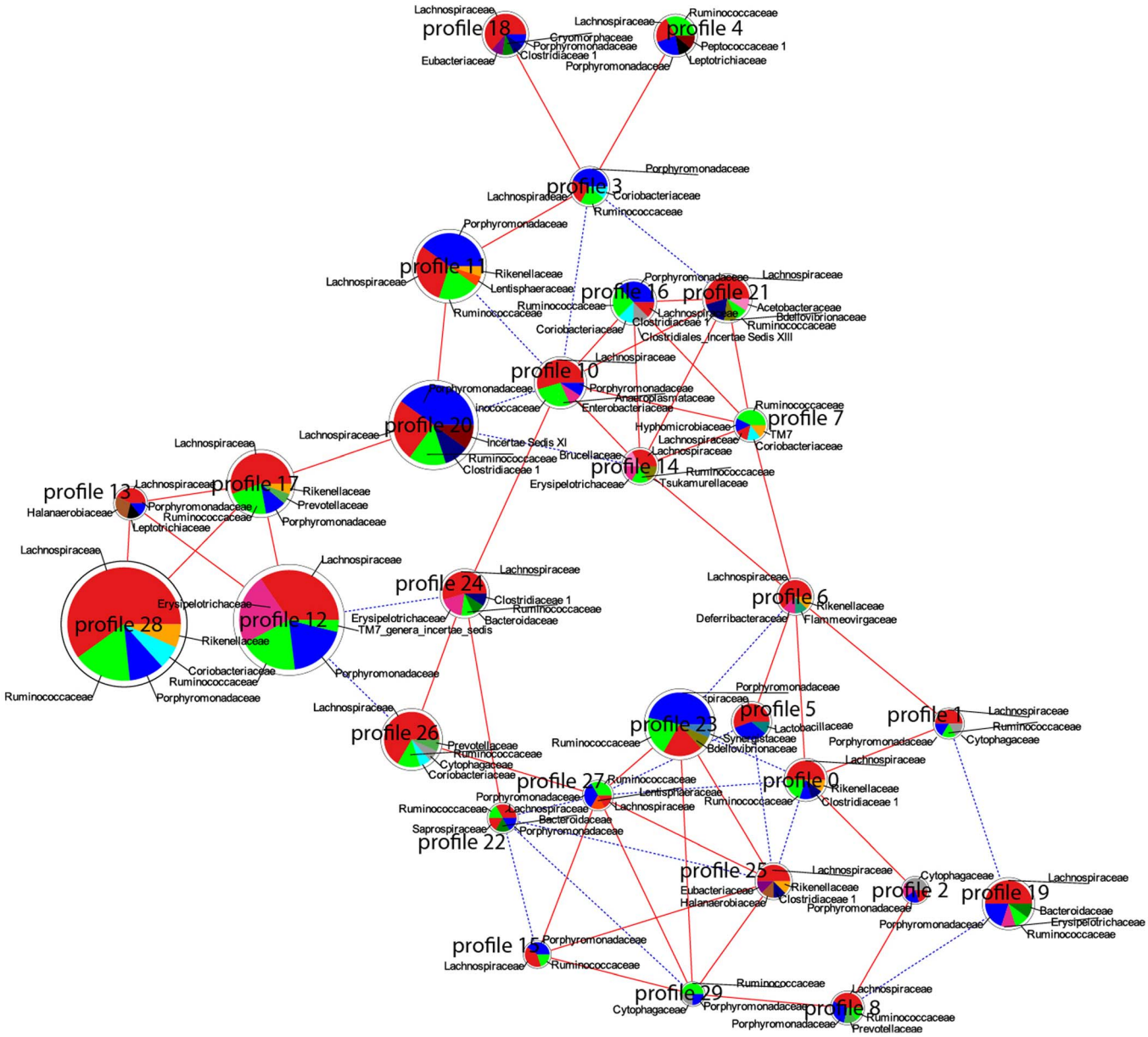

Figure 7 | Microbial network reflects the relationships between the dynamic patterns of OTU profiles and the taxonomic constitution of profiles. Connections indicate positive (red) or negative (blue) correlations (Spearman correlation with P-value < 0.05). The size of each node is proportional to the number of OTUs in the profiles. Pie charts are overlaid on the nodes, representing the abundance of the family-level phylotypes in the profiles.

tively correlated patterns demonstrated different phylotype constitutions, such as profile 20 vs. profile 10 and profile 26 vs. profile 12. This may indicate that bacteria within the same dynamic profile may be grouped together and interact with other groups of bacteria during colitis-induced colorectal carcinogenesis.

Discussion

The gut microbiome is a diverse and complex community whose balance is important for maintaining the healthy state of the host. Colonic dysbiosis is closely related to chronic intestinal inflammation and colorectal cancer[32]. The transition from chronic inflammation to cancer is a multistep process[33], and so the temporal association between the microbiota and disease development is key to understand the pathogenesis. However, there have been few studies that have illustrated this temporal association. In this study, we employed the AOM/DSS murine model for colitis associated colorectal cancer and measured not only the overall shifts of the microbial community but also modifications to the microbiota over time and correlated with molecular changes. We found that microbial community structure was changed by AOM/DSS treatment, and we identified the phylotypes responsible for this change and associated with pathological process. When we generated a longitudinal view of gut microbiota modifications, it was found that phylotypes significantly changed after treatment with different AOM/DSS cycles, and dynamic patterns of the relative abundance of phylotypes were mined.

AOM/DSS treatment exerts toxic effects on the colonic epithelium and alters the colon mucus barrier. AOM can induce DNA mutations and promote epithelial dysplasia. These effects result in intestinal niche alterations and expose the epithelial cells to pathogenic microbes. In accordance with previous reports that employed acute DSS treatment[22,34], we found that the structure of the microbial community was modified by repeated cycles of AOM/DSS treatment. The results showed that community structure was significantly changed,

but community membership was not (Fig. 2A). This indicated that the microbial divergence between AOM/DSS-treated and control mice was obvious in terms of relative abundance shifts of phylotypes but not for the absence or presence of phylotypes. We did not observe significant difference in microbial community structure between mice with inflammation only and mice with tumours. However, this result should be more carefully examined in future studies, as the sample size of these two groups in the current study was relatively small.

At the phylum level, the taxonomic compositions of the gut microbiota are similar between humans and mice. *Bacteroidetes* and *Firmicutes* comprise the largest portion of the entire bacterial community[18]. We observed that the differences at phylum level were not significant. This result is in accordance with acute inflammation animal models[22,34]. However, we found that the average relative abundances of these two phyla in our results (*Bacteroidetes*: 64%–69%, *Firmicutes*: 21%–26%) were different compared with prior studies (*Bacteroidetes*: 21%–31%[22], 0.83%–9.3%[34]; *Firmicutes*: 58%–65%[22], 86%–96%[34]). These differences may be attributed to the animal genetic background and experimental factors such as the location of sampling. The OTUs of the genus *Bacteroides* presented the same variation trends both in our work and in previous report[23]. However, genus *Odoribacter*, which were increased after treatment in previous studies[23], exhibited a divergent change in our work. Genus *Prevotella*, which was decreased after treatment in previous report[23] showed opposite change in our work (Fig. 4B). Comparison of our results with previous reports suggests that the modification of some phylotypes with AOM/DSS treatment may depend on the genetic background of host animals, baseline structure of the microbiota and the AOM/DSS treatment protocols employed.

Correlation analysis of microbial community modification with tumour counts and molecular expression/activity in the molecule network may imply the role of some taxa in the pathological process during colorectal carcinogenesis. For example, OTUs from members of species *Ruminococcus gnavus* were positively related to tumour counts, it implied a tumour promoting effect of the taxon. Accordingly, previous study showed that *R. gnavus* could degrade secretory mucin and were increased in IBD[35]. While OTU00195 from species *Roseburia faecis*,which was negatively related to expressions of COX-2 and p53. *R. faecis* was reported to produce butyrate, a substrate important for maintain normal function of gut epithelium[36]. These results further suggested the intimate connection between bacteria and colitis-associated colorectal cancer; however more studies are still needed to explain underlying mechanisms of the molecule-microbe network for colorectal carcinogenesis.

As the development of colitis-related cancer occurs in a stepwise manner, a time course study is helpful in understanding this process[37]. Longitudinal OTU profiles were mined to describe the dynamic changes in the gut microbiota. The most enriched profile, profile 28, includes OTUs that were first increased and then decreased. These OTUs may be related to t inflammation process. For example, one of these OTUs, OTU00317, from genus *Parabacteroides*, strain from this genus was reported to have anti-inflammation effect[38]. Another profile, profile 10, exhibited a spike after two AOM/DSS cycles just before carcinoma was observed (Fig. 6A). In this profile, OTU02959 (uncl. *Enterobacteriaceae*, BLAST result showed it was from genus *Escherichia*, E-vlaue = 4E-78). One strain in this genus, *Escherichia coli NC101*, was reported to promote carcinoma in a mouse model of chronic colitis[8]. Another genus in profile 10, *Streptococcus*, was also found to be associated with colon cancer[39]. Additionally, we found that the genus *Lactococcus* was significantly enriched in mice treated with 3 and 4 AOM/DSS cycles (Table S4). Both *Lactococcus* and *Streptococcus* are in the same family, *Streptococcaceae*, which was reported to be significantly enriched in human colorectal carcinoma samples[20]. Recently, a bacterial driver–passenger model was proposed for the involvement of the microbiota in colorectal cancer[40]. In this model, bacterial drivers were defined as the bacteria that induced DNA damage and initiated cancer. These bacteria may decrease in abundance after tumour formation, and some bacteria (called passengers in the model) that have a growth advantage can outcompete the drivers. Profile 10 in our result may represent a dynamic pattern of the bacteria drivers.

There are complex interactions among bacteria in gut, and network models effectively descript such interactions[41]. In this work, we utilized dynamic profile clustering technique to explore the structure of microbial community. We found that the profiles were a group of taxa that were closely associated in lineages (Fig. S5 and Table S8). We assumed that taxa in such profiles may form coherent entities and have overlapping niches, just like co-occurring taxa[42]. Taxa in different profiles could interact with taxa in other profiles as a whole, positively or negatively (Fig. 7). Thus, the microbial dysbiosis in colitis related colorectal cancer may be recognized as disorganization of interactions among different groups of taxa rather than individual taxa. But this hypothesis still needs more studies to prove.

In summary, this work investigated the dynamic molecule-microbe networks related to colorectal carcinogenesis. By conducting a longitudinal survey of gut microbiota modifications as well as molecular markers, we revealed a structural shift in the gut microbial community in a mouse model of chronic colitis-associated cancer. In addition to the finding that phylotypes that may play important roles in colitis and cancer and correlate with molecular pathological process, description of the phylotype profiles further provided a comprehensive view of the dynamic changes to the gut microbiota that occur in colitis-associated cancer. This work may offer more information about the role of microbe-host interactions in cancer development.

Methods

Animal experiments. Male BALB/c mice between 6–8 weeks of age were used for experiments. Mice were kept in autoclaved cages and were given sterile food and water. The chronic colitis-to-colitis-associated colorectal cancer murine model was employed based on previous methods[43]. The mice were divided into five groups that received different treatments. Mice in group 1 were given an intraperitoneal injection of AOM (10 mg/kg body weight). One week after the injection, the mice received 3% DSS (molecular weight: 36–50 kDa, Sigma, Germany) in their drinking water for seven days. The mice received another two weeks of sterile drinking water before euthanisation. Mice in group 2 received AOM and two cycles of DSS treatment as described above, mice in group 3 received AOM and three cycles of DSS treatment and mice in group 4 received AOM and four cycles of DSS treatment. Mice in the control group received sterile water before being euthanised. After euthanisation, the colon tissues of the mice were harvested. Tissues were washed with sterile 1× phosphate-buffered saline to collect faecal contents. The colon tissues were fixed in 4% paraformaldehyde for pathological evaluation and immunohistochemistry (IHC). All animal experiments were approved by the Committee for Laboratory Animal Management of Tsinghua University and conducted in accordance with the National Institutes of Health guidelines on the ethical use of animals.

Immunohistochemistry and analysis. IHC was performed using standard protocols. The following antibodies were used: anit-p65 (sc-372, Rabbit, Santa Cruz), anti-PPAR (ZS-72730, Mouse, ZSGB-BIO), anti-p53 (sc-6243, Rabbit, Santa Cruz), anti-COX-2 (sc-376861, Mouse, Santa Cruz). anti-β-catenin (sc-7894, Rabbit, Santa Cruz), anti-CCR2 (ARP 58409-P050, Rabbit, AVIVA SYSTEMS BIOLOGY).

The expression levels of molecules in IHC digital images were quantified by a scoring methods[44]. Breifly, the digital images were processed by a color de-convolution method to separate the DAB and hematoxylin staining. Scores were calculated from the intensity histogram profiles of DAB staining. The trans-nuclear rates of p65 were measured by ImmunoRatio[45].

16S rRNA gene library construction and sequencing. Genomic DNA was extracted and purified with the QIAamp DNA Stool Mini Kit (Qiagen, Hilden, Germany) and used for the preparation of 16S rRNA amplicons. PCR primers targeting the variable V3 region were used to amplify the 16S rRNA (forward primer: 5′-CCTACGGGAGGCAGCAG-3′, reverse primer: 5′-ATTACCGCGGCTGCTGG-3′)[46]. Both primers were added with Illumina paired-end sequencing adapters, and the reverse primer was barcoded with a 6-base code (Table S1). Each reaction mixture contained 25 μL 2× PrimerStar HS Premix (Takara, Dalian, China), 0.5 μL each of the forward and reverse primers (10 μM final concentration), 50 ng template DNA, 0.2 mM dNTPs and 1 U PrimeSTAR HS DNA Polymerase (Takara, Dalian, China) in a final volume of 50 μl. PCR amplification conditions were as follows: denaturation

step at 94°C for 5 minutes, then 25 cycles of 94°C for 45 s, 50°C for 45 s, and 72°C for 60 s, and finally 72°C for 5 min. The amplicons were purified with the QIAquick PCR Purification Kit (Qiagen, Hilden, Germany). 10 control samples and 11 treated samples were randomly assigned to two flow cells of an Illumina MiSeq genome analyser with 151-nucleotide paired-end multiplex sequencing. Human genomic libraries from our own laboratory were mixed with the libraries as controls.

Sequence processing. Sequencing reads were processed with the MiSeq SOP pipeline of the Mothur software package[47,48]. Read pairs were assembled as contigs, and then contigs with ambiguous bases were excluded. The remaining sequences were aligned to the V3 variable region of the 16S rRNA sequences in the Silva database[49], and poorly aligned sequences were removed. Unique sequences were identified, pre-clustered, and screened for chimeras with UCHIME[50]. Sequences were classified with a naive Bayesian classifier, and sequences that did not belong to the bacterial kingdom were excluded (with a 0.8 confidence score). Operational taxonomic units (OTU) that had an average percent identity of 97% were picked from the remaining sequences.

Diversity analysis. Before the diversity analysis, the number of sequences in each sample was normalized by picking the minimum number of sequences of samples (614247 sequences) and randomly selected this number of sequences from each sample. OTU-based analyses of the alpha diversity and beta diversity of the microbial communities were conducted with Mothur. In alpha diversity analysis, rarefaction curves were constructed based on different OTU levels. Chao 1 and ACE were calculated to estimate community richness. The Inverse Simpson index[51] and Shannon index[52] were calculated to estimate community diversity. The Simpson index-based measure and Shannon index-based measure of evenness were calculated to estimate community evenness. In beta diversity analysis, the Jaccard index, Yue & Clayton theta coefficient[53] and Bray-Curtis index[54] were calculated to describe the dissimilarity between microbial communities. The results were visualized with non-metric multidimensional scaling (NMDS). Analysis of molecular variance (AMOVA)[55] was used to test if the dissimilarities between sample groups were significant. Taxonomy classification of OTU was made by the Bayesian classifier in Mothur with the Greengenes database[56] as reference taxonomy.

Identification of differential OTUs. The 'edgeR' package[57] was employed to evaluate the differences in OTU abundance between control mice and all AOM/DSS-treated mice as well as the OTU abundance differences between mice treated with different AOM/DSS cycles. OTUs with very low abundance, which were defined as less than 100 reads, or OTUs that were wholly absent in a total number of samples that was greater than the number of samples in the smallest group for comparison were filtered. For comparison of control and all AOM/DSS treated mice, an exact test[58] was employed; for comparison of control group and groups treated with different AOM/DSS cycles, the generalised linear model likelihood ratio test[59] was performed. Both tests used a threshold of false discovery rate (FDR) < 0.05.

OTU profile clustering and network construction. The Short Time-series Expression Miner (STEM)[60] was used to cluster the OTU relative abundance time course data. The OTUs with very low abundance were filtered as above. The relative abundance of the remaining OTUs was calculated for the STEM input. The maximum number of model profiles was set to 30, and the maximum unit change between time points was set to 2. Significant expression profiles were identified with a false discovery rate of 0.05. A microbial network was constructed to reveal the patterns of similarity/dissimilarity between profiles. Two profiles were connected if the Spearman correlation coefficients of their patterns were significant (P-value < 0.05).

To construct molecule-OTU dynamic networks, the Pearson correlation coefficients between the expression levels scores (trans-nuclear rate for p65) of molecular makers and OTU relative abundances were calculated. The network were constructed by keeping OTUs which at least significantly correlated with one of the six molecular markers (P-value < 0.05). The nodes in the network were coloured according their fold changes comparing to the control group.

1. Trinchieri, G. Cancer and inflammation: an old intuition with rapidly evolving new concepts. *Annu Rev Immunol* **30**, 677–706 (2012).
2. Jess, T., Rungoe, C. & Peyrin-Biroulet, L. Risk of colorectal cancer in patients with ulcerative colitis: a meta-analysis of population-based cohort studies. *Clin Gastroenterol Hepatol* **10**, 639–645 (2012).
3. Ekbom, A., Helmick, C., Zack, M. & Adami, H. O. Increased risk of large-bowel cancer in Crohn's disease with colonic involvement. *Lancet* **336**, 357–359 (1990).
4. Terzic, J., Grivennikov, S., Karin, E. & Karin, M. Inflammation and colon cancer. *Gastroenterology* **138**, 2101–2114 e2105 (2010).
5. Ullman, T. A. & Itzkowitz, S. H. Intestinal inflammation and cancer. *Gastroenterology* **140**, 1807–1816 (2011).
6. Dalton-Griffin, L. & Kellam, P. Infectious causes of cancer and their detection. *J Biol* **8**, 67 (2009).
7. Sears, C. L. *et al.* Association of enterotoxigenic Bacteroides fragilis infection with inflammatory diarrhea. *Clin Infect Dis* **47**, 797–803 (2008).
8. Arthur, J. C. *et al.* Intestinal inflammation targets cancer-inducing activity of the microbiota. *Science* **338**, 120–123 (2012).
9. Qin, J. *et al.* A human gut microbial gene catalogue established by metagenomic sequencing. *Nature* **464**, 59–65 (2010).
10. Littman, D. R. & Pamer, E. G. Role of the commensal microbiota in normal and pathogenic host immune responses. *Cell Host Microbe* **10**, 311–323 (2011).
11. Kamada, N., Seo, S. U., Chen, G. Y. & Nunez, G. Role of the gut microbiota in immunity and inflammatory disease. *Nat Rev Immunol* **13**, 321–335 (2013).
12. Chen, G. Y., Shaw, M. H., Redondo, G. & Nunez, G. The innate immune receptor Nod1 protects the intestine from inflammation-induced tumorigenesis. *Cancer Res* **68**, 10060–10067 (2008).
13. Lowe, E. L. *et al.* Toll-like receptor 2 signaling protects mice from tumor development in a mouse model of colitis-induced cancer. *PLoS One* **5**, e13027 (2010).
14. Wu, S. *et al.* A human colonic commensal promotes colon tumorigenesis via activation of T helper type 17 T cell responses. *Nat Med* **15**, 1016–1022 (2009).
15. Castellarin, M. *et al.* Fusobacterium nucleatum infection is prevalent in human colorectal carcinoma. *Genome Res* **22**, 299–306 (2012).
16. Caporaso, J. G. *et al.* Global patterns of 16S rRNA diversity at a depth of millions of sequences per sample. *Proc Natl Acad Sci U S A* **108 Suppl 1**, 4516–4522 (2011).
17. Jiang, B. *et al.* Integrating next-generation sequencing and traditional tongue diagnosis to determine tongue coating microbiome. *Sci Rep* **2**, 936 (2012).
18. Manichanh, C. *et al.* Reduced diversity of faecal microbiota in Crohn's disease revealed by a metagenomic approach. *Gut* **55**, 205–211 (2006).
19. Frank, D. N. *et al.* Molecular-phylogenetic characterization of microbial community imbalances in human inflammatory bowel diseases. *Proc Natl Acad Sci U S A* **104**, 13780–13785 (2007).
20. Kostic, A. D. *et al.* Genomic analysis identifies association of Fusobacterium with colorectal carcinoma. *Genome Res* **22**, 292–298 (2012).
21. Nell, S., Suerbaum, S. & Josenhans, C. The impact of the microbiota on the pathogenesis of IBD: lessons from mouse infection models. *Nat Rev Microbiol* **8**, 564–577 (2010).
22. Berry, D. *et al.* Phylotype-level 16S rRNA analysis reveals new bacterial indicators of health state in acute murine colitis. *ISME J* **6**, 2091–2106 (2012).
23. Zackular, J. P. *et al.* The gut microbiome modulates colon tumorigenesis. *MBio* **4**, e00692–00613 (2013).
24. Wu, X., Jiang, R., Zhang, M. Q. & Li, S. Network-based global inference of human disease genes. *Mol Syst Biol* **4**, 189 (2008).
25. Rhodes, J. M. & Campbell, B. J. Inflammation and colorectal cancer: IBD-associated and sporadic cancer compared. *Trends Mol Med* **8**, 10–16 (2002).
26. Wolf, M. J. *et al.* Endothelial CCR2 signaling induced by colon carcinoma cells enables extravasation via the JAK2-Stat5 and p38MAPK pathway. *Cancer Cell* **22**, 91–105 (2012).
27. Cui, X. *et al.* Resveratrol suppresses colitis and colon cancer associated with colitis. *Cancer Prev Res.* **3**, 549–559 (2010).
28. Adachi, M. *et al.* Peroxisome proliferator activated receptor γ in colonic epithelial cells protects against experimental inflammatory bowel disease. *Gut* **55**, 1104–1113 (2006).
29. Tanaka, T. Development of an inflammation-associated colorectal cancer model and its application for research on carcinogenesis and chemoprevention. *Int J Inflam* **2012**, 658786 (2012).
30. Suzuki, R., Kohno, H., Sugie, S. & Tanaka, T. Sequential observations on the occurrence of preneoplastic and neoplastic lesions in mouse colon treated with azoxymethane and dextran sodium sulfate. *Cancer Sci* **95**, 721–727 (2004).
31. Ernst, J. & Bar-Joseph, Z. STEM: a tool for the analysis of short time series gene expression data. *BMC Bioinformatics* **7**, 191 (2006).
32. Arthur, J. C. & Jobin, C. The struggle within: microbial influences on colorectal cancer. *Inflamm Bowel Dis* **17**, 396–409 (2011).
33. Fearon, E. R. Molecular genetics of colorectal cancer. *Annu Rev Pathol* **6**, 479–507 (2011).
34. Nagalingam, N. A., Kao, J. Y. & Young, V. B. Microbial ecology of the murine gut associated with the development of dextran sodium sulfate-induced colitis. *Inflamm Bowel Dis* **17**, 917–926 (2011).
35. Png, C. W. *et al.* Mucolytic bacteria with increased prevalence in IBD mucosa augment in vitro utilization of mucin by other bacteria. *Am J Gastroenterol* **105**, 2420–2428 (2010).
36. Louis, P., Young, P., Holtrop, G. & Flint, H. J. Diversity of human colonic butyrate-producing bacteria revealed by analysis of the butyryl-CoA:acetate CoA-transferase gene. *Environ Microbiol* **12**, 304–314 (2010).
37. Bar-Joseph, Z., Gitter, A. & Simon, I. Studying and modelling dynamic biological processes using time-series gene expression data. *Nat Rev Genet* **13**, 552–564 (2012).
38. Kverka, M. *et al.* Oral administration of Parabacteroides distasonis antigens attenuates experimental murine colitis through modulation of immunity and microbiota composition. *Clin Exp Immunol* **163**, 250–259 (2011).
39. Boleij, A., van Gelder, M. M., Swinkels, D. W. & Tjalsma, H. Clinical Importance of Streptococcus gallolyticus infection among colorectal cancer patients: systematic review and meta-analysis. *Clin Infect Dis* **53**, 870–878 (2011).
40. Tjalsma, H., Boleij, A., Marchesi, J. R. & Dutilh, B. E. A bacterial driver-passenger model for colorectal cancer: beyond the usual suspects. *Nat Rev Microbiol* **10**, 575–582 (2012).
41. Faust, K. & Raes, J. Microbial interactions: from networks to models. *Nat Rev Microbiol* **10**, 538–550 (2012).
42. Chaffron, S., Rehrauer, H., Pernthaler, J. & von Mering, C. A global network of coexisting microbes from environmental and whole-genome sequence data. *Genome Res* **20**, 947–959 (2010).

43. Thaker, A. I., Shaker, A., Rao, M. S. & Ciorba, M. A. Modeling colitis-associated cancer with azoxymethane (AOM) and dextran sulfate sodium (DSS). *J Vis Exp* (2012).
44. Chatterjee, S. *et al*. Quantitative immunohistochemical analysis reveals association between sodium iodide symporter and estrogen receptor expression in breast cancer. *PLoS One* **8**, e54055 (2013).
45. Tuominen, V. J., Ruotoistenmaki, S., Viitanen, A., Jumppanen, M. & Isola, J. ImmunoRatio: a publicly available web application for quantitative image analysis of estrogen receptor (ER), progesterone receptor (PR), and Ki-67. *Breast Cancer Res* **12**, R56 (2010).
46. Muyzer, G., de Waal, E. C. & Uitterlinden, A. G. Profiling of complex microbial populations by denaturing gradient gel electrophoresis analysis of polymerase chain reaction-amplified genes coding for 16S rRNA. *Appl Environ Microbiol* **59**, 695–700 (1993).
47. Schloss, P. D. *et al*. Introducing mothur: open-source, platform-independent, community-supported software for describing and comparing microbial communities. *Appl Environ Microbiol* **75**, 7537–7541 (2009).
48. Kozich, J. J., Westcott, S. L., Baxter, N. T., Highlander, S. K. & Schloss, P. D. Development of a Dual-Index Sequencing Strategy and Curation Pipeline for Analyzing Amplicon Sequence Data on the MiSeq Illumina Sequencing Platform. *Appl Environ Microbiol* **79**, 5112–5120 (2013).
49. Quast, C. *et al*. The SILVA ribosomal RNA gene database project: improved data processing and web-based tools. *Nucleic Acids Res* **41**, D590–596 (2013).
50. Edgar, R. C., Haas, B. J., Clemente, J. C., Quince, C. & Knight, R. UCHIME improves sensitivity and speed of chimera detection. *Bioinformatics* **27**, 2194–2200 (2011).
51. Simpson, E. H. Measurement of Diversity. *Nature* **163**, 688 (1949).
52. Krebs & Charles. *Ecological Methodology* (HarperCollins 1989).
53. Yuea, J. C. & Clayton, M. K. A Similarity Measure Based on Species Proportions. *Commun Stat* **34**, 2123 (2005).
54. Bray, J. R. & Curtis, J. T. An ordination of upland forest communities of southern Wisconsin. *Eco Monogr* **27**, 325 (1957).
55. Martin, A. P. Phylogenetic approaches for describing and comparing the diversity of microbial communities. *Appl Environ Microbiol* **68**, 3673–3682 (2002).
56. DeSantis, T. Z. *et al*. Greengenes, a chimera-checked 16S rRNA gene database and workbench compatible with ARB. *Appl Environ Microbiol* **72**, 5069–5072 (2006).
57. Robinson, M. D., McCarthy, D. J. & Smyth, G. K. edgeR: a Bioconductor package for differential expression analysis of digital gene expression data. *Bioinformatics* **26**, 139–140 (2010).
58. Robinson, M. D. & Smyth, G. K. Small-sample estimation of negative binomial dispersion, with applications to SAGE data. *Biostatistics* **9**, 321–332 (2008).
59. McCarthy, D. J., Chen, Y. & Smyth, G. K. Differential expression analysis of multifactor RNA-Seq experiments with respect to biological variation. *Nucleic Acids Res* **40**, 4288–4297 (2012).
60. Ernst, J., Nau, G. J. & Bar-Joseph, Z. Clustering short time series gene expression data. *Bioinformatics* **21 Suppl 1**, i159–168 (2005).

Acknowledgments

We thank Jidong Lang and Jianhuo Fang in center of biomedical analysis, Tsinghua University for sample preparation and sequencing. This work is supported by NSFC grants (91229201 and 81225025) and 973 project (2012CB316504).

Author contributions

S.L. conceived the study. S.L., X.J.L. and H.Y.L. designed the experiments and wrote the manuscript. H.Y.L. established the animal model,collected samples and performed the histological experiments. G.T. constructed th 16S rRNA library and performed sequencing. X.J.L. analyzed the histological and sequencing data. All authors reviewed the manuscript.

Additional information

Supplementary information accompanies this paper at http://www.nature.com/scientificreports

Competing financial interests: The authors declare no competing financial interests.

How to cite this article: Liang, X.J., Li, H.Y., Tian, G. & Li, S. Dynamic microbe and molecule networks in a mouse model of colitis-associated colorectal cancer. *Sci. Rep.* **4**, 4985; DOI:10.1038/srep04985 (2014).